JOURNAL OF AIRCRAFT
Vol. 31, No. 3, May–June 1994

Whirl-Flutter Suppression in Advanced Turboprops and Propfans by Active Control Techniques

F. Nitzsche*
DLR—Institute of Aeroelasticity, D-37073 Göttingen, Germany

The feasibility of using the active control technique to suppress the whirl-flutter instability of advanced turboprops is investigated. Aerodynamic vanes are incorporated at the engine nacelle to generate control airloads. The actuator system is driven by a control law that is based on the Kalman filter estimation of the critical aeroelastic modes of the structure. The results demonstrate that the compensator provides enough controllability to prevent the whirl-flutter onset well beyond the design speed. The present study suggests that a very efficient vibration isolation in advanced turboprops may be achieved both by optimizing the engine-propeller suspension in the actual flying envelope and by employing the active control technique to deal with the safe margins required by the present aircraft certification regulations.

Nomenclature

a = distance between fuselage and nacelle centerlines
b = engine-propeller c.g. distance from pylon elastic axis
c_0, c_c = blade chord, vane chord
d = propeller distance from pylon elastic axis
F = compensator transfer function
G = gyroscopic matrix
$\mathbb{G}_0$, $\mathbb{G}$ = open-, closed-loop transfer function
h = pylon elastic axis flatwise bending displacement
h_y, h_z = aft fuselage cone lateral bending in the horizontal and vertical directions
I_{ph} = propeller polar moment of inertia
I_t = engine-prop moment of inertia about pylon elastic axis
I_x = total polar moment of inertia about fuselage centerline
I_y = engine-prop-nacelle moment of inertia about pylon elastic axis
J^* = propeller advance ratio, $V/\Omega R$
K = closed-loop gain, Fig. 5
K = stiffness matrix
$\mathbb{K}_c$, $\mathbb{K}_f$ = control gain, Kalman filter gain
L_c = vane lift, Fig. 2
l = vane distance from pylon elastic axis
M = mass matrix
M_{y0} = aerodynamic moment about pylon elastic axis
M_0 = mass of aft fuselage cone
m = engine-propeller mass
m_0 = pylon mass
N = number of blades
Q^1, Q^0 = propeller aerodynamic matrices
R^1, R^0 = vane aerodynamic matrices
R = propeller radius
S_c = vane span
t, τ = time
V = freestream airspeed
V_D = aircraft diving speed
v = horizontal displacement of the engine c.g. with respect to the nacelle
w = vertical displacement of the engine c.g. with respect to the nacelle
y, z = engine-propeller total displacements with respect to freestream direction
1, 0 = unit, null matrices
α, β, Γ = compensator design parameters
γ = pylon torsion about elastic axis
ε = vane rotation angle
ζ = aeroelastic mode damping
η = engine-propeller total rotation about pylon elastic axis
θ = torsion angle of aft fuselage cone
ϑ = sensor noise
Λ = matrix of free-vibration eigenvalues
ξ = plant noise
ρ = air density
ϕ = engine-propeller pitch angle
ψ = engine-propeller yaw angle
Ω = propeller spinning frequency
ω = aeroelastic mode frequency
$\omega\chi_j$ = free vibration decoupled natural frequency associated with the dependent variable χ_j

Subscript
1, 2 = powerplants 1 (left) and 2 (right)

Superscripts
* = $(1/\Omega)\partial/\partial t$
$^-$ = nondimensional value
$^\wedge$ = estimated value

Introduction

WHIRL-FLUTTER is an aeroelastic problem described as an oscillatory instability of the engine-propeller installation. Two-degree-of-freedom models, for which the engine-propeller structure is considered to be a rigid body free to develop only the pitch and yaw natural modes with respect to the airstream direction, are able to reproduce the precessional motion that may become unstable under certain conditions.[1] In the classical whirl-flutter analysis the flexibility of the system is supposed to be defined by a combination of the individual flexibilities due to both the engine suspension (or shock mounting system) and the backup structure that supports it. The mass properties are lumped at the engine-propeller c.g., yielding a simplified dynamic system that can reliably analyze the phenomenon in structures where the interaction is negligible between the aforementioned pitch and yaw modes, and the natural modes associated with the

Presented as Paper 91-122 at the DGLR/AAAF/RAES/AIAA International Forum on Aeroelasticity and Structural Dynamics, Aachen, Germany, June 3–6, 1991; received Sept. 11, 1991; revision received April 15, 1993; accepted for publication May 19, 1993.

*Scientist, Bunsenstraße 10. Member AIAA.

backup structure. In modern configurations of turboprops, where pusher propeller engines are supported by short pylons cantilevered with the aft fuselage cone (Fig. 1), the whirl-flutter analysis requires more elaborate work.[2,3] Considerable influence of the backup structural dynamics is observed, and a coupling between the two powerplants leads to the development of both symmetric and antisymmetric whirl-flutter conditions, in many cases involving a major participation of the supporting structure. Furthermore, as opposed to the classical whirl-flutter phenomenon, the instability may become violent and cannot be suppressed by passive means such as flutter dampers.

The present work extends a previous study on the feasibility of applying the active control technique to both suppress whirl-flutter and improve low-frequency vibration transmissibility characteristics from the powerplants to the structure of such advanced turbopropeller configurations.[4] In the preliminary phase of the design, the engine suspension specialist faces the well-known problem of selecting a shock mounting system that cuts off the unpleasant forced vibrations generated by the propellers and withstands a single structural failure. The optimization of such a design often deals with two reverse trends. A suspension which is efficient in terms of transmissibility is likely to be characterized by the "soft" spring rates that are prone to generate unstable situations, especially in the event of a shock mount failure. Hence, the active control may be employed either to stabilize the system in the dangerous conditions determined by a structural failure or to provide an extra safety margin to the nominal design at higher speeds.

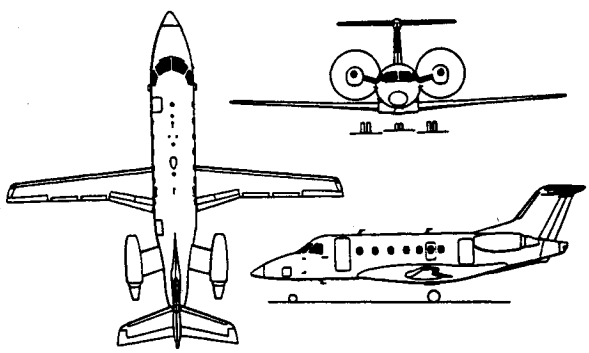

Fig. 1 Pusher configuration.

Feasibility

A pair of aerodynamic vanes is designed at the two nacelles to achieve controllability of the system. The vanes are positioned at a distance l from the pylon elastic axis, according to Fig. 2. The goal is to provide—through appropriate angular displacements of the two vanes—the aerodynamic forces that can control both the pylon bending and the pylon torsion, precluding symmetric and antisymmetric whirl-flutter conditions. The control philosophy, although simple, is efficient if the critical aeroelastic mode presents significant displacements of the pylon elastic axes. This is not an abnormal situation, and it is prone to occur in any advanced turboprop configuration.[3] The magnitude of the aerodynamic moments generated by the vane and the propeller at the pylon elastic axis are estimated, respectively

$$M^c_{y_0} = (\tfrac{1}{2})\rho V^2 S_c c_c l(2\pi\varepsilon) \tag{1}$$

$$M_{y_0} = (c_0/2)R(4N\Omega^2R^2m_a/c_0^2)A'_2\phi \tag{2}$$

Equation (2) is reproduced from Ref. 2, with

$$m_a = \rho(\pi c_0^2/4)R \tag{3}$$

$$A'_2 = (\tfrac{1}{2})J^{*2}[\sqrt{1+J^{*2}} - J^{*2}\log(1+\sqrt{1+J^{*2}}/J^*)] \tag{4}$$

Hence, the ratio between the two aerodynamic moments may be calculated, yielding

$$M^c_{y_0}/M_{y_0} = f(J^*)\nu\bar{l} \tag{5}$$

where $f(J^*)$ is presented in Fig. 3 and

$$\nu = c_cS_c/(Nc_0R) \tag{6}$$

Equation (5) indicates that the efficiency of the control is proportional to the parameters ν (the ratio between the area of the vanes and the area of the blades) and the nondimensional distance between the pylon elastic axis and the vane hinge. According to Fig. 3, $f(J^*)$ is approximately 10 for $J^* = 1.5$; therefore, the ratio between the two moments in Eq. (5) approaches the unity when the product $\nu\bar{l} \simeq 0.1$. Since $J^*_{cr} = 1.13$ for the open-loop design,[4] the numerical values of ν and $\bar{l}$ assumed in Table 1 are expected to satisfy the present investigation.

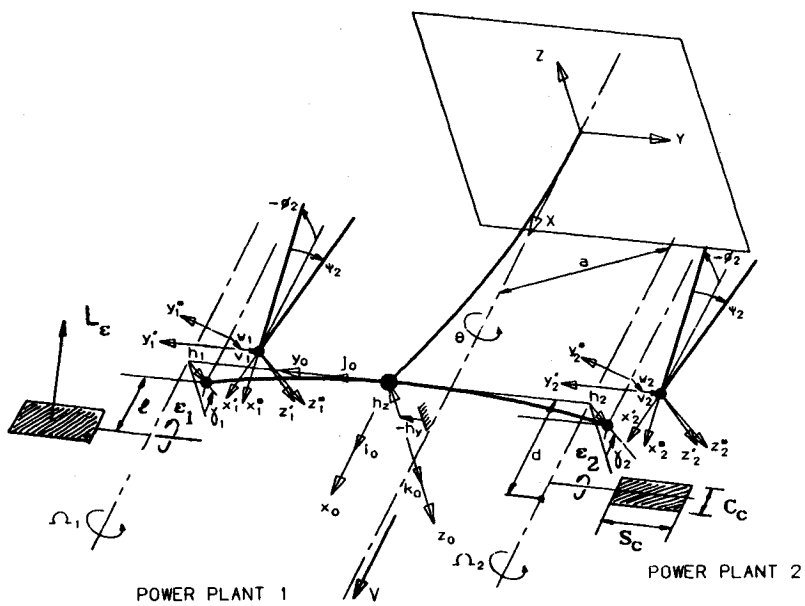

Fig. 2 Aerodynamic control vanes.

Table 1 Definition of the aeroservoelastic system[a]

$\bar{a} = 1.6216$	$\bar{I}_j = 0.0355$
$\bar{b} = 0.2008$	$\bar{I}_y = 0.0390$
$\bar{d} = 0.7876$	$\bar{I}_x = 1.030$
$\bar{c}_0 = 0.1961$	$\bar{I}_{ph} = 0.0033$
$\bar{c}_c = 0.2317$	$\bar{\omega}_{\psi_1} = \bar{\omega}_{\psi_2} = 0.3816$
$\nu = 0.0760$	$\bar{\omega}_{\phi_1} = \bar{\omega}_{\phi_2} = 0.2167$
$\bar{l} = 0.3861$	$\bar{\omega}_{v_1} = \bar{\omega}_{v_2} = \bar{\omega}_{w_1} = \bar{\omega}_{w_2} = 1.681$
$\mu = 0.0013$	$\bar{\omega}_{\gamma_1} = \bar{\omega}_{\gamma_2} = 1.796$
$\Omega_1 = 178$ rad/s	$\bar{\omega}_{h_1} = \bar{\omega}_{h_2} = 0.1685$
$\Omega_2 = -178$ rad/s	$\bar{\omega}_y = 0.0823$
$\bar{m} = 0.1353$	$\bar{\omega}_z = 0.0628$
$\bar{m}_0 = 0.0109$	$\bar{\omega}_\theta = 0.0600$

[a]The geometric properties are nondimensionalized by R; the mass properties by the system total mass; the moment-of-inertia properties by the system total mass $\times R^2$; and the frequency properties by Ω.

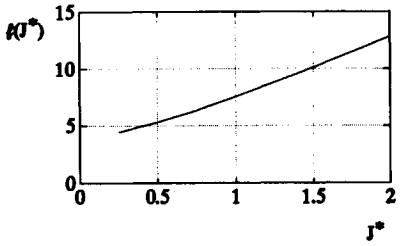

Fig. 3 Vane/propeller aerodynamic-moment ratio vs J^*.

Reduced-Order Aeroservoelastic Equations

The equations of motion of the aeroservoelastic system for the full-state feedback idealization were already developed in a former study.[4] Here, these equations are written in a slightly different form, assuming that the control variables (provided by the aerodynamic vanes) are decoupled from the system's state variables. This assumption holds if the poles associated with the control system are well separated from the poles that characterize the backup structure and the engine-propeller suspension. Since the whirl-flutter phenomenon is prone to occur in the lower frequency range, involving low-damped structural modes, the latter assumption is the same as considering that the control system is "fast enough" and able to generate instantaneous airloads.

The 15 coupled, second-order, linear differential equations that describe the system's dynamics are cast in the state vector form:

$$\overset{*}{\boldsymbol{x}} = \boldsymbol{Ax} + \boldsymbol{Bu} \tag{7}$$

where

$$\boldsymbol{A} = \begin{bmatrix} M^{-1}\begin{bmatrix}\mu(Q^1 + \nu R^1) - G \\ 1\end{bmatrix} & M^{-1}\begin{bmatrix}\mu(Q^0 + \nu R^0) - K \\ 0\end{bmatrix} \end{bmatrix} \tag{8}$$

$$\boldsymbol{B} = \begin{bmatrix} \mu\nu M^{-1}S \\ 0 \end{bmatrix} \tag{9}$$

$$\boldsymbol{u} = [\varepsilon_1^c \varepsilon_2^c]^T \tag{10}$$

$$\boldsymbol{x} = [\overset{*}{\boldsymbol{q}}\boldsymbol{q}]^T \tag{11}$$

$$\boldsymbol{q} = [\psi_1 \bar{v}_1 \bar{h}_y \bar{v}_2 \psi_2 \phi_1 \gamma_1 \bar{h}_1 \bar{w}_1 \bar{h}_z \theta \bar{w}_2 \bar{h}_2 \gamma_2 \phi_1]^T \tag{12}$$

$$\mu = 2N\bar{m}_a/\bar{c}_0 \tag{13}$$

When the above equations are compared with those presented in Ref. 4, it is worthwhile to point out that the dependence of the airloads on the time derivatives of the vane angle of attack is now neglected ($\overset{*}{\varepsilon}_1^c = \overset{*}{\varepsilon}_2^c = 0$ and $S = S^0$), and thus, ν is factored out from matrices R^1 and R^0.

The modal superposition technique is employed in order to reduce the order of the aeroservoelastic system

$$\boldsymbol{x} = \tilde{\Phi}\chi; \qquad \tilde{\Phi} = \text{block diagonal } (\Phi) \tag{14}$$

where Φ is the modal matrix of the related free-vibration eigenproblem, truncated after m significant natural modes. Hence

$$(-\omega_i^2 M + K)\Phi_i = 0, \qquad i = 1, 2, \ldots, m \tag{15}$$

where ω_i and Φ_i are the ith eigenfrequency and related eigenvector, respectively. Using the normalization

$$\Phi^T M \Phi = 1 \Rightarrow \Phi^T K \Phi = \Lambda \tag{16}$$

the equations of motion may be rewritten as

$$\overset{*}{\chi} = \mathcal{A}\chi + \mathcal{B}\boldsymbol{u} \tag{17}$$

where

$$\mathcal{A} = \begin{bmatrix} \mu(\mathcal{Q}^1 + \nu\mathcal{R}^1) - \mathcal{G} & \mu(\mathcal{Q}^0 + \nu\mathcal{R}^0) - \Lambda \\ 1 & 0 \end{bmatrix} \tag{18}$$

$$\mathcal{B} = \begin{bmatrix} \mu\nu\mathcal{S} \\ 0 \end{bmatrix} \tag{19}$$

$$\begin{bmatrix} \mathcal{Q} \\ \mathcal{R} \\ & \mathcal{G} \end{bmatrix} = \tilde{\Phi}^T \begin{bmatrix} Q \\ & R \\ & & G \end{bmatrix} \tilde{\Phi} \qquad \mathcal{S} = \Phi^T S \tag{20}$$

According to Fig. 4, the superposition of three natural modes is capable of reproducing the critical whirl-flutter condition. These modes are referred to as numbers 9, 10, and 12 in Table 2. Figure 4 also plots the result obtained using only the two most important natural modes (numbers 9 and 10). The latter approximation yields good agreement for the damping at $J^* = J^*_{cr}$, but for $J^* < J^*_{cr}$ accuracy is lost. An additional result, obtained with the superposition of modes including the gyroscopic effect, is depicted in Fig. 4. These special coordinates ("gyro coords") also generate accurate results, but not superior to those obtained with the three natural modes.

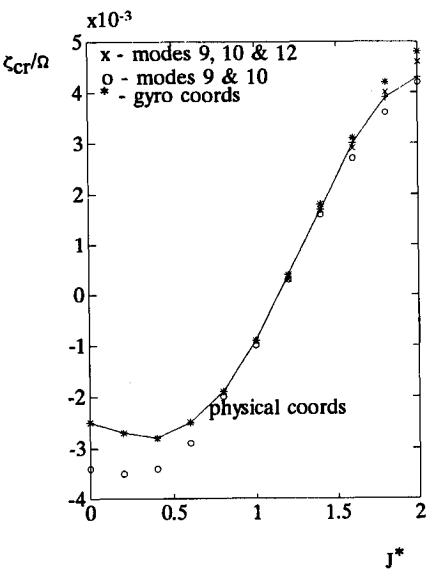

Fig. 4 Critical aeroelastic mode description in truncated coordinates: ζ_{cr}/Ω vs J^*.

Table 2 Open-loop free-vibration eigenvalues $J^* = 0$; $\rho = 0$ kg/m^3; $\Omega_1 = 178$ rad/s; $\Omega_2 = -178$ rad/s

Mode no.	ω/Ω	ζ/Ω
01	4.9928	0
02	4.9888	0
03	4.6721	0
04	4.6721	0
05	1.6400	0
06	1.4346	0
07	0.9300	0
08	0.6027	0
09[a]	0.5981	0
10[b]	0.5357	0
11	0.4598	0
12[c]	0.4157	0
13	0.2828	0
14	0.2298	0
15	0.2053	0

[a]Antisymmetric propeller yaw.
[b]Symmetric pylon bending-torsion and propeller pitch.
[c]Symmetric fuselage cone vertical bending and propeller pitch.

For the sake of simplicity, the superposition of the natural modes (listed at the bottom of Table 2) was considered sufficient.

Optimum Compensator Design

The optimum compensator design will be based on the linear quadratic Gaussian (LQG) technique, for which both the aeroservoelastic equations in modal coordinates

$$\overset{*}{\chi} = \mathcal{A}\chi + \mathcal{B}\boldsymbol{u} + \xi(t) \tag{21}$$

and the output equations

$$\iota = \mathcal{C}\chi + \mathcal{D}\boldsymbol{u} + \vartheta(t) \tag{22}$$

are perturbed by white-noise functions. Thus, the control problem resumes in minimizing a cost function $\mathcal{J}$, involving both the system and the control states

$$\mathcal{J} = \mathcal{E}\int_0^\infty [\chi^T \boldsymbol{u}^T]\begin{bmatrix}\mathbb{Q} & \\ & \mathbb{R}\end{bmatrix}\begin{bmatrix}\chi \\ u\end{bmatrix} dt \tag{23}$$

subject to Eqs. (21) and (22). The plant and sensor uncorrelated noises satisfy the expected-value function:

$$\mathcal{E}\left[\begin{bmatrix}\xi(t) \\ \vartheta(t)\end{bmatrix}[\xi(t)^T\vartheta(t)^T]\right] = \begin{bmatrix}\Gamma\Xi & 0 \\ 0 & \Theta\end{bmatrix}\delta(t-\tau) \tag{24}$$

In the present formulation

$$\mathbb{Q} = \alpha\begin{bmatrix}1 & \\ & \Lambda\end{bmatrix} \quad \text{and} \quad \mathbb{R} = \beta 1 \tag{25}$$

Hence, the quadratic forms $\chi^T\mathbb{Q}\chi$ and $u^T\mathbb{R}u$ become proportional to 1) the kinetic and potential energies (in modal coordinates); and 2) the work done by the control vanes, respectively. A suitable combination of α, β, and Γ will select the compensator's "best design."

The full-state control law

$$\boldsymbol{u} = -\mathbb{K}_c\hat{\chi} = -(1/\beta)\mathcal{B}^T\mathbb{P}\hat{\chi} \tag{26}$$

(where $\mathbb{P}$ is the solution of the algebraic Riccati equation associated with the LQG problem), is realized through a Kalman filter modal-state estimation. For this, the dynamics of the estimator is considered, yielding

$$\overset{*}{\hat{\chi}} = \mathcal{A}\hat{\chi} + \mathcal{B}\boldsymbol{u} + \mathbb{K}_f(\iota - \mathcal{C}\hat{\chi} - \mathcal{D}\boldsymbol{u}) \tag{27}$$

If two vanes are used in the control and three natural modes are superimposed to generate the whirl-flutter critical mode, the size of the vectors $\boldsymbol{u}$ and ι in Eq. 22 are 2×1 and 6×1, respectively. Therefore, the design of the compensator is generally defined by a multiple-input, multiple-output (MIMO) control problem. However, due to the system's symmetry properties, it is verified that the whirl-flutter onset may only occur in either a symmetric or an antisymmetric aeroelastic mode.[3] Since the control law is synthesized to suppress a pre-established critical condition for which its characteristics are a priori known, one of the following relationships must hold: $\varepsilon_1^c = \varepsilon_2^c$ or $\varepsilon_1^c = -\varepsilon_2^c$. The problem becomes single-input, multiple-output (SIMO). In this particular example, the latter relationship holds as long as the critical mode is symmetric.

The next simplification, to a single-input, single-output (SISO) problem, relies upon the hypothesis that the aeroelastic response at the whirl-flutter onset condition may be dominated by a *single aeroelastic mode*. Indeed, since such a mode is much less damped at the vicinity of the critical speed, it generates a very strong output. Assuming that the SISO hypothesis is true, it is feasible to construct the matrix $\mathcal{C}$ in Eq. (22) using the participation coefficients of the natural modes in the critical aeroelastic mode defined by the open-loop analysis. The contribution of the remaining aeroelastic modes to the total aeroelastic response at the critical condition may be incorporated into the noise associated with the sensor $\vartheta(t)$. The validity of the SISO hypothesis will be checked later in this work, based on a full-state simulation of both the control law and the Kalman filter gain.

Placement of Poles of the Closed-Loop System

The system's closed-loop block diagram is depicted in Fig. 5. The transfer function between the plant noise and the aeroelastic response is

$$\iota(s) = (1 + \mathrm{K}\mathbb{G}_0F)^{-1}\mathbb{G}_0\xi(s) = \mathbb{G}\xi(s) \tag{28}$$

where

$$\iota(s) = [\mathcal{C}(1s - \mathcal{A})^{-1}\mathcal{B} + \mathcal{D}]\boldsymbol{u}(s) = \mathbb{G}_0\boldsymbol{u}(s) \tag{29}$$

In a first compensator design no feed-forward path between $\boldsymbol{u}(s)$ and $\iota(s)$ will be considered. This is equivalent to set $\mathcal{D} = 0$ in Eq. (22). The white-noise correlation matrices in Eq. (24) are selected based on a robustness criterion: controllers incorporating a high level of uncertainty can withstand larger variations from the design values without degrading their performance. Therefore, assuming that 20% of the aeroelastic modal response at the whirl-flutter onset is represented by the sensor white noise

$$\Theta = 0.20\mathcal{C}\mathcal{C}^T \tag{30}$$

Next, it is assumed that the plant white noise can be as large as the input control

$$\Xi = \mathcal{B}\mathcal{B}^T \tag{31}$$

In a stationary random process, the mean-square time-histories of both the state and the control variables may be readily estimated.[5] These are calculated at a design point which is set immediately beyond the whirl-flutter open-loop critical advance ratio ($J^*_{\mathrm{des}} = 1.2$, $J^*_{\mathrm{cr}} = 1.13$, respectively). For $\alpha = 1$, Figs. 6a and 6b present the variation of a) the root-mean-square (rms) value of the composed pitch-yaw pro-

peller angle, $\sigma_{rms} = \sqrt{\phi^2_{rms} + \psi^2_{rms}}$ vs β; and b) the rms value of the vane angle of attack vs β. Three curves are shown for different levels of plant noise ($\Gamma = 10^{-1}$, 10^{0}, and 10^{1}, respectively). As expected, when increasing the relative cost of the control (represented by β), ε^c_{rms} decreases, whereas σ_{rms} increases. Moreover, increasing the level of the plant noise (represented by Γ), σ_{rms} and ε^c_{rms} also increase. Figures 7a and 7b are plotted vs β, showing a) the negative of the critical aeroelastic mode damping; and b) the value of the cost function

$$\mathcal{J} = \chi_0 \mathbb{P} \chi_0^T \tag{32}$$

(where the initial conditions are set assuming $\chi_0 = 1$, arbitrarily). Figure 7a recovers the classic result that the complex poles of the unstable open-loop system converge to their mirror images as the cost of the control approaches infinity.[6]

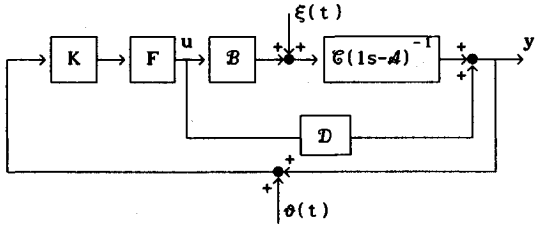

Fig. 5 Closed-loop system block-diagram.

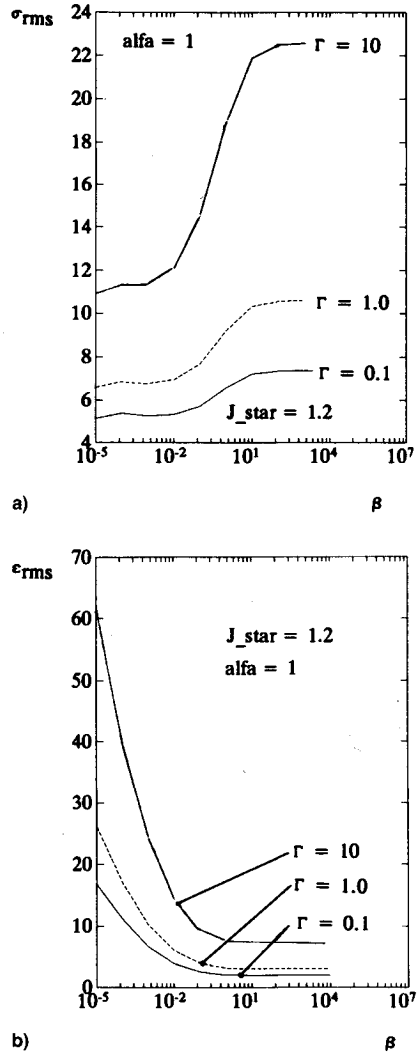

Fig. 6 Compensator design: a) σ_{rms} vs β and b) ε^c_{rms} vs β for Γ = 10^{-1}, 1 and 10.

Figure 7b indicates that larger values of β lead to bad controller designs, as long as $\mathcal{J}$ also increases indefinitely.

Thus, it is estimated from Figs. 6 and 7 that $\alpha = 1$, $\beta = 0.01$, and $\Gamma = 1$ lead to a feasible design, for which the results of Table 3 are true. The selected values of α, β, and Γ are substituted into Eq. (28), and the closed-loop system characteristics are calculated (Table 4).

A second compensator design, including the information on the vane's angle of attack in the controller feed-forward path, was also studied. A constant gain, $\mathcal{D} = 0.01$, was assumed. The performance of the latter design compared to the previous one is evaluated in the following.

Control System Robustness

Table 5 gives the poles and transmission zeros of the open-loop transfer function obtained from Eq. (27). Since the system being studied is one of a nonminimum phase, with poles and zeros in the unstable region, the controller may at most be conditionally stable. In order to verify its robustness, an arbitrary gain was introduced in the block diagram of Fig. 5. Figures 8a and 8b indicate that the robustness associated with the two controllers designed ($\mathcal{D} = 0$ and $\mathcal{D} = 0.01$) is more than adequate, but also similar. Gain margins based on the closed-loop transfer function return difference[6]

$$T(s) = 1 + \mathrm{K}\mathbb{G}_0(s)F(s) \tag{33}$$

of 41 and 46 dB ($0.391 < \mathrm{K} < 110$ and $0.391 < \mathrm{K} < 194$, at $J^*_{des} = 1.2$) are obtained for the two designs, respectively.

Table 3 Closed-loop design values

$\mathcal{J} = 412$
$\sigma_{rms} = 6.95$ deg
$\varepsilon_{rms} = 6.14$ deg
$\mathbb{K}_c = (-1.224 \quad -13.34 \quad 3.874 \quad 4.387 \quad -0.1707 \quad -0.1421)$
$\mathbb{K}_f = (0.8202 \quad -0.3883 \quad 0.01672 \quad 0.3788 \quad 1.672 \quad -0.1309)^T \times 10^3$

Table 4 Characteristic values of $\mathbb{G}$; $J^* = 1.2$; $\mathcal{D} = 0$; $K = 1$

Zeros	Poles
$+0.0127 \pm 0.0641i$	$-0.0218 \pm 0.6249i$
$-0.0147 \pm 0.4384i$	$-0.0064 \pm 0.4454i$
$-1.816 \pm 0.0000i$	$-0.0008 \pm 0.5506i$
$-0.0220 \pm 0.6249i$	$-0.0221 \pm 0.6249i$
$-0.0053 \pm 0.5506i$	$-0.0041 \pm 0.5506i$

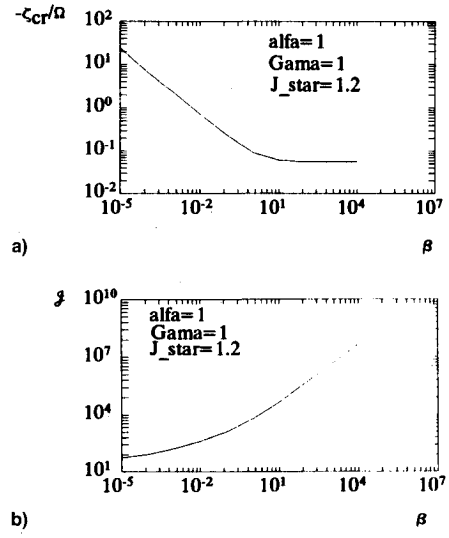

Fig. 7 Compensator design: a) $-\zeta_{cr}/\Omega$ vs β and b) $\mathcal{J}$ vs β for Γ = 1.

Table 5 Characteristic values of $\mathbb{G}_0$; $J^* = 1.2$; $\mathfrak{D} = 0$

Transmission zeros	Poles
$+0.0127 \pm 0.6041i$	$-0.0218 \pm 0.6249i$
$-0.0147 \pm 0.4384i$	$+0.0003 \pm 0.5506i$
$-1.816 \pm 0.0000i$	$-0.0064 \pm 0.4454i$

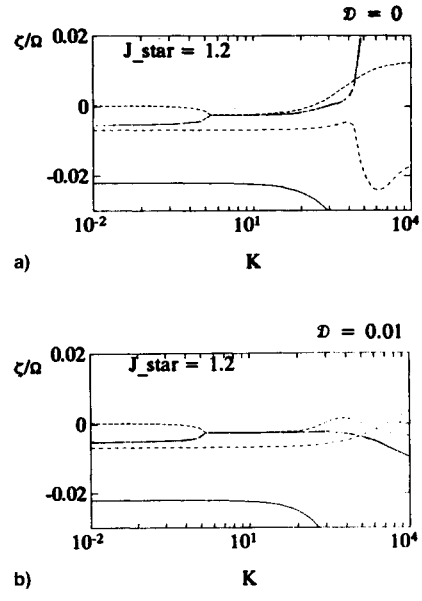

Fig. 8 Compensator robustness: ζ/Ω vs K: a) $\mathfrak{D} = 0.0$ and b) $\mathfrak{D} = 0.01$.

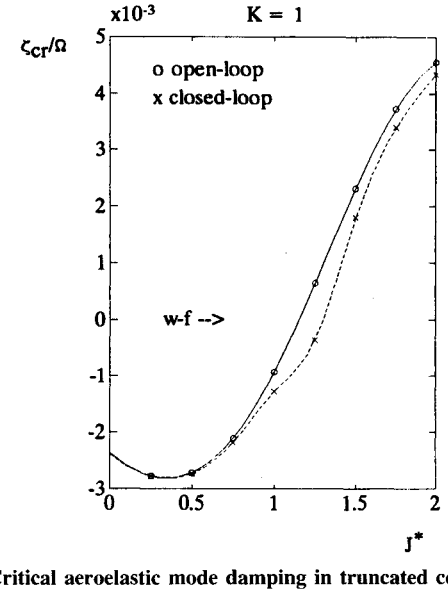

Fig. 9 Critical aeroelastic mode damping in truncated coordinates: ζ_{cr}/Ω vs J^* for the open- and closed-loop conditions.

Closed-Loop System Performance

Figure 9 presents a plot of the critical mode damping ratio as a function of J^* for the open- and closed-loop conditions ($\mathfrak{D} = 0$ is taken thereafter for the sake of design simplicity). The controller prevents the whirl-flutter onset from $J^*_{cr} = 1.13$ (open-loop) up to $J^*_{cr} = 1.28$, corresponding to a 13.6% gain in aircraft velocity. However, the performance of both the control law and the Kalman filter in the presence of the whole set of modes remains questionable. To accomplish this analysis, Eq. (26) is substituted into Eqs. (7), (22), and (27). Next, Eq. (22) [with $\vartheta(t) = 0$] is further substituted into Eq.

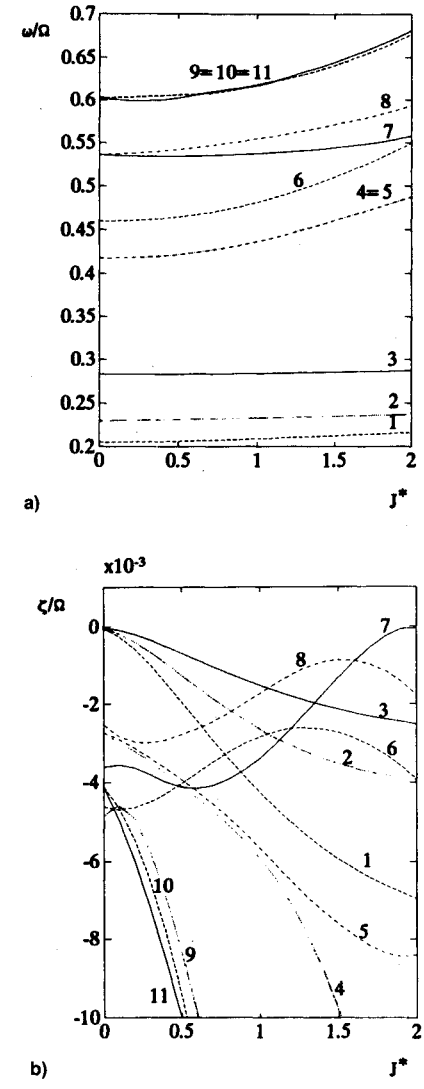

Fig. 10 Closed-loop system: root-locus vs J^* in physical coordinates ($K = 1$ and $\mathfrak{D} = 0.0$). For better identification, the plot only depicts the first 11 most significant aeroelastic modes: a) ω/Ω vs J^* and b) ζ/Ω vs J^*.

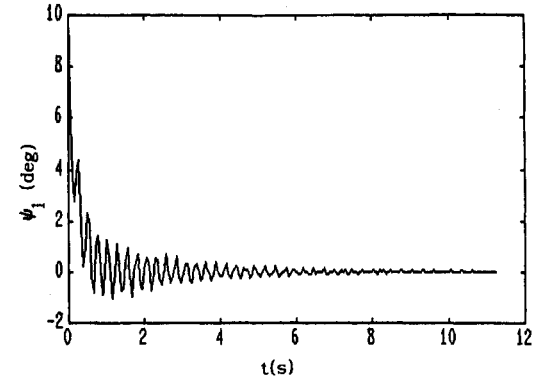

Fig. 11 Active control time-domain simulation for the initial condition $\psi_1 = \psi_2 = 10$ deg: ψ_1 vs t.

(27). After the transformations between physical and modal coordinates are performed

$$\begin{bmatrix} x \\ \hat{\chi} \end{bmatrix}^* = \begin{bmatrix} A & -\tilde{\Phi}\mathcal{B}\mathbb{K}_c \\ \mathbb{K}_f\mathcal{C}\tilde{\Phi}^T & \mathcal{A} - \mathcal{B}\mathbb{K}_c - \mathbb{K}_f\mathcal{C} \end{bmatrix} \begin{bmatrix} x \\ \hat{\chi} \end{bmatrix} \tag{34}$$

The characteristic roots of Eq. (34) are plotted in Figs. 10a and 10b vs J^*. The root loci indicate that no instability occurs

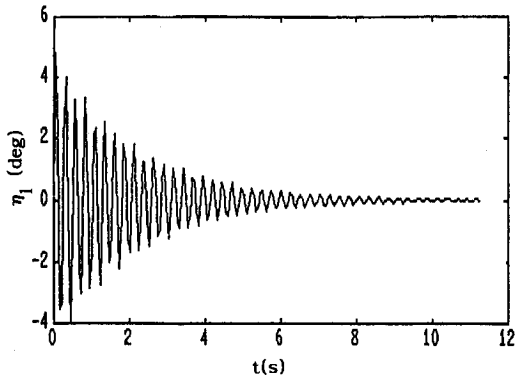

Fig. 12 Active control time-domain simulation for the initial condition $\psi_1 = \psi_2 = 10$ deg: η_1 vs t.

up to $J^*_{cr} = 2.0$, when mode 7 becomes marginally stable. Hence, the compensator has a superior performance in the presence of all aeroelastic modes.

$$y = \begin{bmatrix} y_1 \\ y_2 \\ \psi_1 \\ \psi_2 \\ z_1 \\ z_2 \\ \eta_1 \\ \eta_2 \end{bmatrix} = \begin{bmatrix} \bar{d} & 1 & -1 & 0 & 0 & & & & & & & & \\ 0 & 0 & -1 & 1 & \bar{d} & & & & & 0 & & & \\ 1 & 0 & 0 & 0 & 0 & & & & & & & & \\ 0 & 0 & 0 & 0 & 1 & & & & & & & & \\ & & & & & -\bar{d} & -\bar{d} & 1 & 1 & -1 & \bar{a} & 0\ 0 & 0 & 0 \\ & & & 0 & & 0 & 0 & 0 & 0 & -1 & -\bar{a} & 1\ 1 & -\bar{d} & -\bar{d} \\ & & & & & -1 & -1 & 0 & 0 & 0 & 0 & 0\ 0 & 0 & 0 \\ & & & & & 0 & 0 & 0 & 0 & 0 & 0 & 0\ 0 & -1 & -1 \end{bmatrix} q \tag{A1}$$

In the Appendix, the output vector describing the aeroelastic response is written as a function of the dependent variables [see Appendix, Eq. (A1)]. Figures 11 and 12 depict time domain simulations of the most interesting components of y when both propellers are submitted to an initial condition given by a symmetric yaw angle of 10 deg at $J^*_{des} = 1.2$. These results indicate that the system reaches its steady-state value in about 6 s if the control law is also activated at $t = 0$.

Conclusions

A simple control system for whirl-flutter suppression and critical modal damping augmentation is demonstrated to be feasible. The estimated performance of the compensator, designed in the reduced modal space, is even better when the complete set of the eigenvectors of the structure is included.

The merit of this investigation is clear when the current FAR-JAR/Part 25 regulations for aircraft certification are invoked. According to these requirements, the aircraft shall be free from any structural instability up to 1) $1.2V_D$ in the nominal configuration; and 2) $1.0V_D$ under a single structural failure. Often, the transmissibility characteristics of the shock mount system are downgraded in favor of the required safety margin. The present study proposes that the safety margins can be reached by *active control*. In this case, the controller could be activated *outside* the boundaries of the flying envelope of the aircraft, and no special redundancies should be done with respect to the fail-safeness of the controller itself. Such an approach would allow significant improvements in the design of efficient engine suspension systems. They could be optimized within the flying envelope, and no additional stiffness would be necessary to accommodate eventual shock mount failure.

Appendix: Aeroelastic Response—Output Vector

In a former study,[2] the total displacements of the propeller with respect to the undisturbed airflow direction were calculated as a function of the dependent variables of the aeroelastic system q. These are the four linear displacements of the two propeller hubs with respect to the equilibrium position: y_1 and y_2 (lateral) and z_1 and z_2 (vertical); and the related angular displacements: ψ_1 and ψ_2 (yaw) and η_1 and η_2 (pitch). They are related to the output of the system according to the following relationship:

Acknowledgments

The present investigation was partially supported by the Brazilian Government through CNPq—Conselho Nacional de Desenvolvimento Científico e Tecnológico. Acknowledgments are also due to EMBRAER—Empresa Brasileira de Aeronáutica, where most of the present investigation was developed.

References

[1]Houbolt, J. C., and Reed, W. H., III, "Propeller-Nacelle Whirl-Flutter," *Journal of the Aerospace Sciences*, Vol. 29, No. 3, 1962, pp. 333–346.

[2]Nitzsche, F., "Whirl Flutter Investigation on an Advance Turboprop Configuration," *Journal of Aircraft*, Vol. 26, No. 10, 1989, pp. 939–946.

[3]Nitzsche, F., "Insights on the Whirl-Flutter Phenomena of Advanced Turboprops and Propfans," *Journal of Aircraft*, Vol. 28, No. 7, 1991, pp. 463–470.

[4]Nitzsche, F., "Whirl-Flutter Suppression in Advanced Turboprops and Propfans by Active Control Techniques," *Proceedings of the 17th International Council of the Aeronautical Sciences (ICAS '90)*, Vol. 1, Stockholm, Sweden, Sept. 1990, pp. 419–426.

[5]Bryson, A. E., Jr., and Ho, Y.-C., *Applied Optimal Control*, Hemisphere, New York, 1975, pp. 408–437.

[6]Friedland, B., *Control System Design: An Introduction to State-Space Methods*, McGraw-Hill, New York, 1986.